Resonance Ionization of Titanium: High Useful Yield and New Autoionizing States

Journal:	*Journal of Analytical Atomic Spectrometry*
Manuscript ID	JA-ART-08-2018-000269.R1
Article Type:	Paper
Date Submitted by the Author:	07-Sep-2018

Complete List of Authors:	Trappitsch, Reto; Lawrence Livermore National Laboratory, Nuclear and Chemical Sciences Division Savina, Michael; Lawrence Livermore National Laboratory, Nuclear and Chemical Sciences Division Isselhardt, Brett; Lawrence Livermore National Laboratory, Nuclear and Chemical Sciences Division

Journal Name

ARTICLE TYPE

Cite this: DOI: 10.1039/xxxxxxxxxx

Resonance Ionization of Titanium: High Useful Yield and New Autoionizing States

Reto Trappitsch,*[a] Michael R. Savina,[a] and Brett H. Isselhardt[a]

Received Date
Accepted Date

DOI: 10.1039/xxxxxxxxxx

www.rsc.org/journalname

The isotopic composition of titanium in meteoritic phases can be used to decipher processes such as stellar nucleosynthesis and galactic chemical evolution. In order to facilitate analyses of trace amounts of titanium in atom-limited samples, we established a new three-step resonance ionization scheme. The scheme was developed using titanium-sapphire lasers and we show that it can be easily saturated and that it yields stable isotope measurements. Using the LION (Laser Ionization Of Neutrals) instrument we demonstrate a useful yield of $10.1\% \pm 1.6\%$ when ionizing from the ground state. We determined the population of two low-lying electronic states within the ground state multiplet and show that accessing all three levels of the ground state manifold would result in an overall useful yield of $\sim 18\%$. The useful yield agrees well with expectations based on prior analyses of uranium using LION. In addition, we report the energy levels of nine new autoionizing states between 56217 cm^{-1} and 57086 cm^{-1}.

1 Introduction

Titanium is the 21st most abundant element in the universe and is important when studying stellar nucleosynthesis as well as galactic chemical evolution. Titanium is a lithophile refractory element and has a 50% condensation temperature* of 1582 K.[1,2] Due to this high condensation temperature, titanium is expected to readily condense into presolar stardust grains. These are grains that condensed in the outflow of dying stars, were transported through the interstellar medium, and incorporated into meteorite parent bodies at the formation of the Solar System.[3,4] Each presolar grain records the nucleosynthetic fingerprint of its parent star and can thus be used to study stellar nucleosynthesis. However, low-mass stars ($\lesssim 8$ solar masses) do not significantly influence the isotope abundances of elements like titanium, chromium, iron, and nickel. Dust grains from such stars thus preserve the isotopic abundances of many of these elements prior to the parent star formation, which significantly pre-dates the Solar System. Analyzing presolar grains from such stars can thus yield valuable insight into the workings of galactic chemical evolution.[5–7]

Because presolar stardust grains are small (of order micrometer in diameter), their analysis requires techniques with high spatial resolution and sensitivity, especially when analyzing trace element isotopic compositions. While titanium can be analyzed in these grains by NanoSIMS, a secondary ion mass spectrometry (SIMS) technique with a sub-micrometer spatial resolution, the whole sample usually needs to be consumed due to the low useful yield† of this technique.[5,8] Reported useful yields for SIMS measurements when sputtering on a glass standard range between 0.03% and $\sim 3\%$ for high and low energy secondary ions, respectively.[9] Real world samples that are not in an oxide matrix and for which the high energy secondary ions are analyzed to avoid molecular interference will have useful yields that are closer to the low side of this range. Resonance ionization mass spectrometry (RIMS) on the other hand has a much higher useful yield and has been successfully applied to study multi-element isotopic abundances in presolar grains.[7,10,11] An additional advantage of RIMS over other techniques is the suppression of interfering isobars. While titanium has been previously analyzed by RIMS,[12,13] these studies used dye lasers for resonance ionization with wavelengths that cannot be easily reached using newer titanium-sapphire (Ti:Sa) laser cavities.[14,15]

Here we present a new three photon, three color resonance ionization scheme for titanium, which we developed using the LION (Laser Ionization Of Neutrals) instrument.[16] We first briefly review the laser and mass spectrometry setup[16] and then present the scheme and the associated spectroscopy of neutral titanium atoms. We show that our three step scheme can be easily satu-

[a] Nuclear and Chemical Sciences Division, Lawrence Livermore National Laboratory, 7000 East Ave, L-231, Livermore, CA 94551.
* Corresponding author, trappitsch1@llnl.gov

* The 50% condensation temperature is defined as the temperature at which 50% of the element is condensed into the solid phase assuming a gas of solar composition and a total pressure of 10^{-4} bars.

† We define useful yield as the ratio of the number of atoms detected to the number consumed during the analysis of a given sample.

rated with Ti:Sa lasers and provides stable and consistent isotopic results with a high useful yield.

2 Methods

2.1 Samples

Two different materials were analyzed in this study, namely titanium metal and a National Institute of Standards and Technology (NIST) standard reference material (SRM) 1264a. Both samples were polished prior to loading them into the instrument. The titanium metal was used to develop the resonance ionization scheme. We used the SRM 1264a standard in order to identify potential isobaric interferences. This standard is a high-carbon steel with a certified‡ titanium abundance of 0.24%. Elements that have atomic isobars with titanium isotopes are Ca, V, and Cr, which occur in SRM 1264a with abundances of 0.00004%, 0.10%, and 0.06%, respectively.

2.2 Instrumentation

All RIMS measurements were done on the LION instrument at Lawrence Livermore National Laboratory. In brief, sample material was sputtered using a pulsed 15 keV Ga^+ ion beam with variable pulse length. This ion pulse is created by a fine-focus IonOptika liquid metal ion gun, and the primary beam, which has an incident angle of 60° with respect to the normal of the sample, was rastered over the sample surface with a 10-25 μm square raster. After the ion pulse, secondary ions are ejected from the system (unless otherwise noted). The neutral titanium atoms are then resonantly ionized with three tunable Ti:Sa lasers (pulse widths around 10-20 ns) as described in Section 3.1. Ions are subsequently extracted into a time-of-flight mass analyzer and separated by their mass-to-charge ratios, before being detected in ion counting mode on a MagnetTOF discrete dynode detector. The laser pulses and data acquisition is run at 1 kHz repetition rate. The chamber base pressure for all presented measurements was around 2×10^{-8} mbar. Details on RIMS and the LION instrument as well as on measurement evaluation have been previously published and the reader is referred to this literature.[7,15,16]

2.3 Surface cleaning procedures

Multiple methods are available to clean the sample surface prior or during RIMS analysis.[17] This cleaning is done to remove the oxide layer that builds up over time on a pristine titanium surface and to keep the sample from reoxidizing in between analysis shots. From an oxide free surface we expect to mostly sputter titanium neutral atoms, which can be subsequently ionized resonantly by the Ti:Sa lasers. From an oxidized surface however, much of the material will sputter as TiO, which is not effectively ionized by the lasers and will thus be lost from the analysis, effectively reducing the useful yield.

When analyzing a sample, the ion beam is removing material from the surface for only a fraction of the total analysis time. A common primary ion pulse length for analysis is 200 ns, which results in a duty cycle of 0.2% for a 1 kHz repetition rate. Ion extraction and detection is actually turned off during most of this time; the main reason to limit the repetition rate to 1 kHz is that the Ti:Sa lasers decrease in power per pulse for higher repetition rates. Since no ion detection takes place, the Ga^+ beam can be turned on in between measurements for a given amount of time to keep the sample surface reduced for the next measurement. This allows us to achieve stable count rates from shot to shot, which is especially important for doing laser spectroscopy and measuring saturation curves.

In addition to the Ga^+ ion gun, LION is equipped with a Hiden IG20 gas ion gun that can be used to clean / pretreat the analysis surface with various ions.[17] The incident angle of these ions is 60° with respect to the normal of the sample. We used this gun to sputter clean the analysis surface with 3 keV Ar^+ ions. Alternatively, the surface was pre-sputtered with Ga^+ ions in continuous mode prior to analysis. While the Ar^+ ion beam is $> 100\,\mu$m diameter on the sample surface and thus several times larger than the Ga^+ beam used for analysis, the Ar^+ beam current was several orders of magnitude higher. Surface cleaning can therefore be achieved in a short amount of time. While cleaning with the Ga^+ beam implants Ga ions into the sample matrix, effectively changing the sample composition, the Ar^+ gun allows cleaning without significant change to the sample composition.

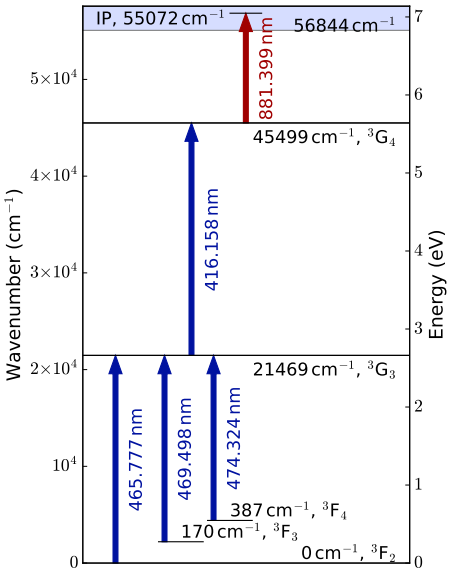

Fig. 1 Schematic drawing of the developed titanium resonance ionization scheme.

3 Results

3.1 Titanium resonance ionization scheme

Figure 1 shows the resonance ionization scheme for neutral titanium, including the autoionizing (AI) transition. The ground state of titanium is $^3F_2$ and is part of a multiplet with a $^3F_3$ state at 170 cm^{-1} and a $^3F_4$ state at 387 cm^{-1}. Using the atomic spec-

‡ The certificate can be found on the NIST website: https://www-s.nist.gov/srmors/certificates/1264A.pdf

tra database from NIST[§], we selected a $^3G_3$ state at 21469 cm^{-1} as the first excited state, which can be accessed from all states in the ground state multiplet. From this state we connect further to a $^3G_4$ state at 45499 cm^{-1}, which was chosen such that the angular momentum change (ΔJ) of the transition is +1, which is ideal since it minimizes the odd-even effect (see Section 4.3). The ionization potential (IP) for titanium is at 55072 cm^{-1} and the selected AI state found in this work (Section 3.3), is at 56844 cm^{-1}.

We performed wavelength scans and saturation curves for all transitions in Figure 1. Throughout this manuscript we identify the resonance ionization scheme by the term symbol for the lowest state. The second and third step of the resonance ionization scheme were always the ones shown in Figure 1, unless otherwise noted.

3.2 Wavelength scans of the 1st and 2nd transitions

Figure 2 shows wavelength scans for the transitions $^3F_2 \rightarrow {}^3G_3$ and $^3G_3 \rightarrow {}^3G_4$. These scans were performed at laser irradiances that clearly saturated the transitions (see Section 3.4). The full width at half maximum (FWHM) of the $^3F_2 \rightarrow {}^3G_3$ transition is $\sim$ 18 pm while the FWHM of the $^3G_3 \rightarrow {}^3G_4$ transition is $\sim$ 39 pm. The center wavelengths of the transitions are exactly as the values calculated from the literature and are the same for all titanium isotopes, i.e., we did not observe any isotope specific wavelength shifts. This finding is likely due to our laser bandwidth of 10 – 15 pm, which is large compared to typical titanium isotope shifts of 0.5 to 1.5 pm[13].

We did not perform wavelength scans for the transitions starting on the $^3F_3$ and $^3F_4$ state and assume that the calculated wavelengths are correct for these transitions as well. This is a reasonable assumption. The levels are well known and we did not observe any discrepancies between the above measured transitions and their calculated wavelengths.

3.3 Autoionizing transitions

An ionization step to excite the neutral titanium atom from the $^3G_3$ state at 45498.815 cm^{-1} over the ionization potential (IP) at 55072.5 cm^{-1} is required. Ionization generally requires a significantly higher irradiance for saturation than the other steps. We

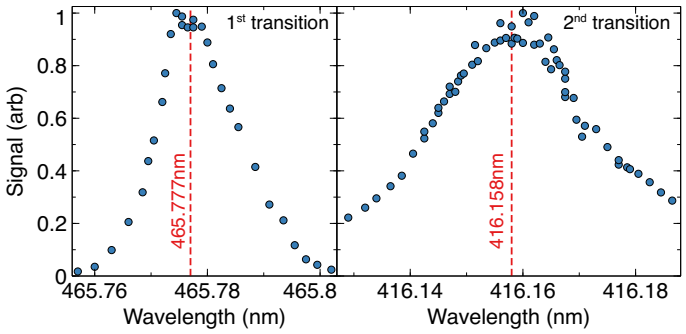

Fig. 2 Wavelength scans of the $^3F_2 \rightarrow {}^3G_3$ and $^3G_3 \rightarrow {}^3G_4$ transitions.

§ https://www.nist.gov/pml/atomic-spectra-database

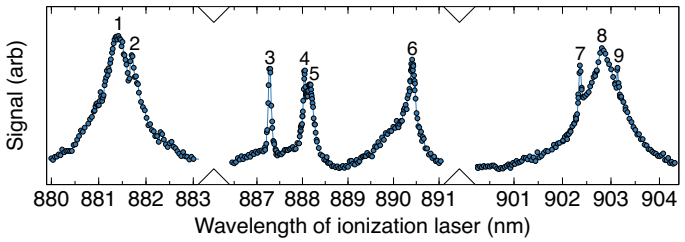

Fig. 3 Wavelength scans showing titanium AI states accessible from the $^3G_4$ state at 45499 cm^{-1}.

scanned the region between 56217 cm^{-1} and 57086 cm^{-1} (between 933 nm and 863 nm) to find AI transitions that can be saturated with our Ti:Sa laser. Preliminary scans indicated three regions with broad spectral features, between 880 – 883 nm, between 886.5 – 891 nm, and between 901 – 904 nm. Figure 3 shows subsequent detailed scans of these regions. We scanned with stepsizes $\leq$ 20 pm and reduced the stepsize as necessary, e.g., around the center of peaks. We discovered nine peaks, which are labeled in Figure 3. Note that the absolute peak heights in the figure cannot be compared, since some of the transitions may be saturated while others may not. Table 1 gives the levels and wavelengths for all AI transitions as well as the approximate peak widths.

The ideal AI transition is saturated and gives a stable, unfractionated isotope signal. We found that the transition to the AI state at 56844.4 cm^{-1} can be easily saturated (see Section 3.4) and gives stable isotope ratios without significant fractionation (see Section 4.3).

3.4 Saturation curves

Figure 4 shows saturation curves for transitions originating on the two lowest levels of the ground state multiplet, as well as the second bound-bound transition and the AI transition. The ion signals are normalized to the maximum signals. The red lines are fits to a first-order rate model:[18]

$$N = N_i + N_{max} \cdot \left[1 - \exp\left(-\frac{I}{I_{sat}}\right)\right] \quad (1)$$

Here N is the measured signal, N_i the measured signal at zero irradiance, N_{max} the maximum signal, I the laser irradiance, and I_{sat} the saturation irradiance of the transition. While this model does not describe real multilevel transitions, it provides a semi-quantitative measure of the effectiveness of the schemes.

As Figure 4 shows, the three transitions in the scheme that

Table 1 Discovered AI transitions and associated levels.

Peak No.	Level (cm^{-1})	Wavelength (nm)	Peak width (pm)
1	56844.4	881.399	600
2	56840.6	881.697	40
3	56769.2	887.281	70
4	56759.5	888.047	80
5	56758.0	888.16	230
6	56729.6	890.409	230
7	56580.9	902.358	60
8	56575.2	902.82	700
9	56571.4	903.13	100

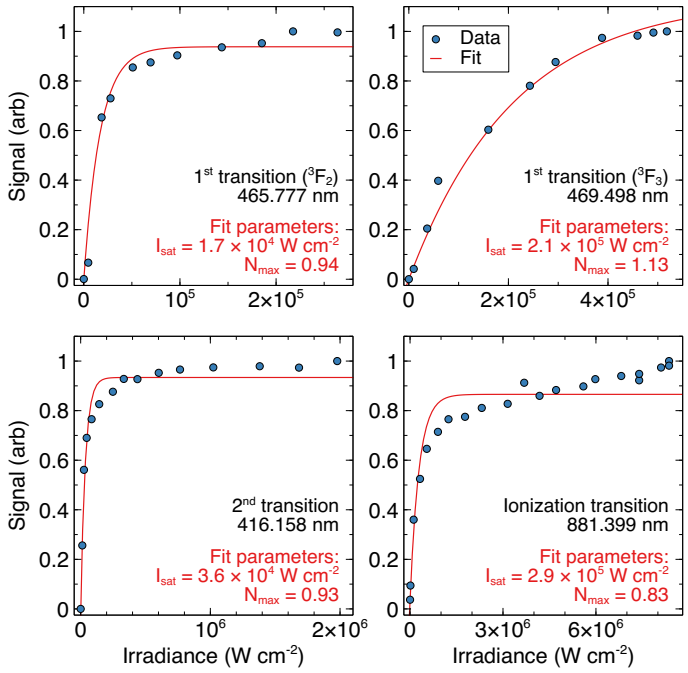

Fig. 4 Saturation curves of all saturated transitions.

starts on the $^3F_2$ ground state are saturated; the fitted N_{max} is < 1 for these transitions indicating that a different effect increases the signal beyond the maximum signal in a first-order rate model. The slow increase in signal beyond saturation, which can especially be seen in the ionization transition, is likely due to an increase in effective laser volume with increasing laser power. The Ti:Sa laser profiles are roughly Gaussian. Increasing the laser power thus increases the possibility to ionize neutrals that are further out in the laser volume, i.e., in the wings away from the center line. This will slowly increase the signal as seen in the figure and is not accounted for in equation (1). Figure 4 shows that N_i is ~ 0 for all transitions, i.e., that all lasers are required in order to ionize titanium. Thus we do not observe alternate ionization processes such as two-color three-photon ionization in which a second photon from one of the first two lasers causes ionization (bypassing the AI step).

The first transition from the low-lying excited $^3F_3$ state is saturated, however the fit shows that we can expect up to 13% more signal with increased power. Figure 5 shows the saturation curve for the first transition from the $^3F_4$ state. This transition is obviously not saturated, in fact, the signal rise is exponential. The fit to this curve has the functional form of $N = a \cdot I^b$. Here N is the signal, I the set irradiance, and a and b are fitting parameters. While a is simply a scaling parameter, b has a value of 1.2 and is an indicator of the photon order of the $^3F_4 \rightarrow {}^3G_3$ transition. A single photon process, i.e., one photon exciting the atom to the next state from which it will then be independently excited until ionized, would depend linearly on the irradiance ($b = 1$). A fractional exponent greater than one indicates multiple ionization mechanisms. The poor fit at high irradiance likely indicates that the relative contributions of the mechanisms are changing.

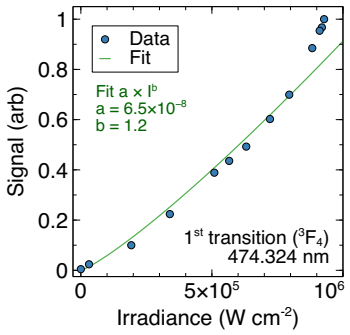

Fig. 5 Saturation curve of the unsaturated $^3F_4 \rightarrow {}^3G_3$ transition.

3.5 Useful yield and ground state multiplet population

To determine the useful yield, the titanium sputter rate from the metal sample when sputtering with 15 keV Ga^+ needs to be known. Using a continuous gallium beam, we sputtered five $20 \times 20\,\mu$m pits into the polished titanium metal standard. The volume of each crater was then determined by optical interferometry (ZeGage, Zygo Corp.), allowing us to calculate how many titanium atoms were removed from the sample. By using the measured beam current and the time used to sputter each crater we calculated an average titanium sputter yield per incident Ga^+ ion of 4.3 ± 0.7. The uncertainty here is simply the standard deviation of the five individual measurements.

To determine the useful yield, we first cleaned the sample surface to remove the top TiO_x layer using 3 keV Ar^+. We subsequently sputtered and measured 10000 mass spectra, each using a 175 ns long Ga^+ pulse for sputtering sample material. During the total measurement time of 10 s the surface does not significantly reoxidize and thus allows measuring an accurate value for the highest achievable useful yield. This highest achievable yield was $10.1\% \pm 1.6\%$ for ionization from the $^3F_2$ ground state and $5.6\% \pm 0.8\%$ for ionization from the $^3F_3$ state. Since the transition from the $^3F_4$ state was not saturated (see Section 3.4), we did not determine the useful yield for the scheme that originated on that state.

In order to determine the ideal delay time between the primary ion pulse and the laser ionization pulse, i.e., to ensure optimal overlap of the expanding plume of neutral atoms and the ionization lasers, we determined useful yields for the scheme starting

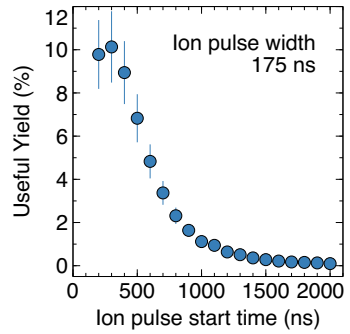

Fig. 6 Useful yield measurements depending on various ion pulse delay times.

on the $^3F_2$ state for various ion pulse delay times. Figure 6 shows the results of this study. In order to facilitate the shortest delay time, we turned the secondary ion ejection voltage pulse off. In practice, we observed negligible titanium secondary ion signals from clean metal surfaces. Figure 6 shows that the optimal delay time is 200-300 ns.

4 Discussion

4.1 Isobaric supression

One of the key advantages of RIMS over other techniques is the suppression of interfering isobars, which generally do not get efficiently ionized by the lasers. Potential isobaric interferences exist on ^{46}Ti from ^{46}Ca, on ^{48}Ti from ^{48}Ca, and on ^{50}Ti from ^{50}Cr and ^{50}V. In order to determine the respective suppression factors, we measured the NIST 1264a standard, which has known abundances for these potentially interfering elements (see Section 2.1). In a 1.7 h long measurement collecting 6×10^6 mass spectra, we detected a total of 391128 counts of titanium, but no counts of calcium, vanadium, or chromium above background. Assuming that the concentration of Ca:Ti:V:Cr is 1:1:1:1 in a given sample and assuming solar isotopic composition[2] we calculated lower limit suppression factors based on the non-detection of the potentially interfering species. These suppression factors are given in Table 2. It is likely that they are several orders of magnitude higher, as, e.g., previously determined for nickel.[7] By using SRM 1264a, it is however not feasible to measure the actual suppression values due to the low abundances of the elements of interest in the standard and the random background in the mass channels of interest. Even for high-precision RIMS measurements with uncertainties of a couple of permil, as e.g., achieved by Boehnke *et al.*,[19] the suppression factors shown in Table 2 are already high enough if titanium is not a minor element compared to the potential interferences.

4.2 Excited state populations

Figure 7 shows the relative populations within the ^{3}F multiplet. We fitted a Boltzmann distribution to the first two states in order to estimate the population of the $^3F_4$ state, which could not be saturated by our setup and for which the actual population could thus not be experimentally determined. Since the three states are all part of the same multiplet we expect that can be described by a Boltzmann distribution.[20] Using this extrapolation, we determined that the sputtered neutral titanium occupies the $^3F_2$, $^3F_3$, and $^3F_4$ states at levels of 55%, 31%, and 14%, respectively. Compared to the study by Dullni,[20] the $^3F_2$ state shows a higher population in our study. We calculated a population temperature from

Table 2 Lower limits for isotopic suppression factors for the interfering isotopes assuming equal sample concentration for all elements and solar isotopic composition.

Ti isotope	Interfering isotope	Isobaric suppression
^{46}Ti	^{46}Ca	$> 1.6 \times 10^5$
^{48}Ti	^{48}Ca	$> 3.0 \times 10^4$
^{50}Ti	^{50}V	$> 3.2 \times 10^6$
^{50}Ti	^{50}Cr	$> 3.4 \times 10^3$

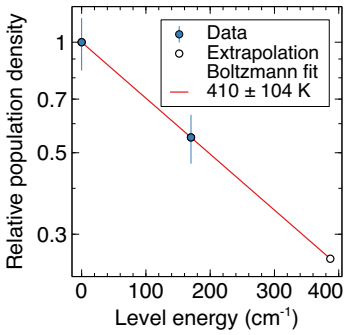

Fig. 7 Boltzmann fit used to determine the relative population of the $^3F_4$ state.

the Boltzmann distribution[20,21] of 410 ± 104 K (1σ). Dullni[20] determined a population temperature of 700 ± 140 K for sputtering titanium from an oxygen free titanium metal surface and a population temperature of 1400 ± 400 K for sputtering from a oxidized surface. The population temperature obtained in this study for a reduced titanium metal hence is lower than the previously determined value,[20] uncertainties on both values are however rather large.

Figure 8 shows decreasing signal for both the $^3F_2$ and $^3F_3$ states with time as an Ar^+-cleaned surface sits in vacuum. We attribute this to loss of neutral titanium to TiO_x in the sputtered flux. Since TiO_x is not ionized by our lasers we cannot confirm that this is so, however the effect is observed for uranium metal[22] where UO_x is observed to increase in RIMS spectra as the surface oxidizes. Furthermore, TiO_x rises sharply in SIMS spectra when clean titanium metal is exposed to oxygen.[23] Dullni[20] exposed titanium metal to oxygen and observed a loss of $^3F_2$ titanium in the sputtered flux, which was attributed to sputtering titanium as Ti^+ and TiO_x rather than neutral titanium. At our chamber pressure of 2×10^{-8} mbar the arrival rate of O_2 from the gas phase is $\sim 1.6 \times 10^{-3}$ monolayers per second. Thus we expect monolayer coverage in ~ 600 s. This is roughly the time required for the signal in Figure 8 to decay to half its initial value, and further decrease is extremely slow. This behavior is consistent with loss of metallic titanium to surface oxidation.

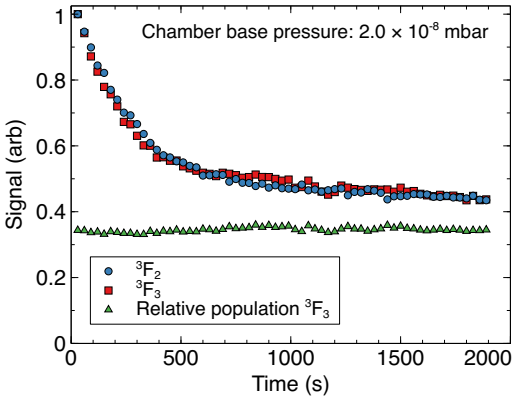

Fig. 8 Reoxidization curves for Ar^+-cleaned titanium metal for the $^3F_2$ and $^3F_3$ states as well as their relative occupancy.

The two decay curves in Figure 8 were not measured simultaneously; rather we measured them subsequently in exactly same way with the same Ar^+ cleaning procedure prior to measurement and no Ga^+ cleaning between analysis cycles. We assume that the oxidation rate was the same for the two measurements since multiple reoxidization curves in this and other studies[17] showed no differences when keeping the experimental conditions the same.

Figure 8 shows that the relative populations of the two states do not change with the oxidization state of the surface. Other authors have noted sharp changes in the relative populations of electronic states when metallic surfaces oxidize,[20,22,24,25] however this occurs only when the states belong to different multiplets. In the present case, both probed states are part of the same multiplet. Dullni[20] observed only a small shift in relative populations within the titanium ^{3}F multiplet, which was attributed to a difference in the kinetic energy distribution of the departing atoms from a metallic versus oxidized surface (i.e., a difference in the Boltzmann temperature). Hayashi and Kubota[24] showed that the relative populations of states within two different multiplets of iron do not change significantly with surface oxidation. Our result agrees with these earlier studies.

4.3 Isotope ratios

There are five stable titanium isotopes with solar abundances of 8.249% for ^{46}Ti, 7.437% for ^{47}Ti, 73.72% for ^{48}Ti, 5.409% for ^{49}Ti, and 5.185% for ^{50}Ti.[2] Figure 9 shows the measured isotope ratios normalized to ^{48}Ti as δ-values, which are permil deviations from the expected isotopic compositions of the sample, which we assume to be solar. The measurements originating from the $^3F_2$ state show little isotopic fractionation. The titanium resonance ionization scheme that starts from the $^3F_3$ state however does show a clear enhancement in the odd isotopes of +164‰ and +156‰ in ^{47}Ti and ^{49}Ti, respectively. These differences were calculated between the measurements to avoid mass fractionation that is not due to the odd-even effect itself.

These various isotopic fractionations are due to differences in the angular momenta between the $^3F_2$ and $^3F_3$ states. Angular momentum selection rules dictate that the achievable ionization efficiencies are different, even for saturated transitions. Linearly polarized light interacting with even isotopes allows transitions between magnetic substates m_j when $\Delta m_j = 0$. The transition $m_0 \rightarrow m_0$ is however forbidden when $\Delta J = 0$, but allowed when $\Delta J = \pm 1$. The $m_0 \rightarrow m_0$ transition is always allowed for odd isotopes due to the magnetic moment of the nucleus breaking the degeneracy of the m_j states. These selection rules lead to different expected fractionations between the two resonance ionization schemes since the transition $^3F_2 \rightarrow {}^3G_3$ is $\Delta J = +1$ while the transition $^3F_3 \rightarrow {}^3G_3$ is $\Delta J = 0$. It is thus possible to ionize all titanium isotopes equally well when originating from the $^3F_2$ state, however only six out of the seven m_j of the even titanium isotopes are connected to the $^3G_3$ state when originating on the $^3F_3$ state. We would thus expect that the isotope fractionation is +167‰ for the odd isotopes in the scheme originating on the $^3F_3$ state, which is close to what we observed (Figure 9).

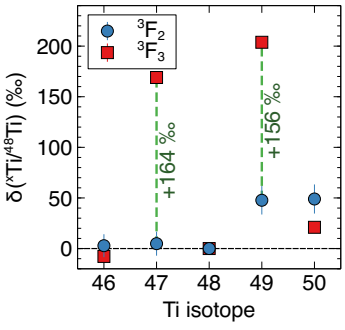

Fig. 9 Isotope ratios measured for the fully saturated schemes originating on the $^3F_2$ and $^3F_3$ states. A clear odd-even effect can be seen in the latter scheme.

Since we observe minimal odd-even effect in the overall resonance ionization scheme starting on the $^3F_2$, we can use the angular momentum selection rules to specify that the ionizing transition from the $^3G_4$ state to the AI state is $\Delta J = \pm 1$. The AI state at 56844.4 cm^{-1} thus has angular momentum of $J = 3$ or $J = 5$. For the other AI states (Table 1) we cannot rule out $\Delta J = 0$ for the transition since we did not measure isotope ratios or saturation curves.

4.4 Comparison of useful yield with previous studies

In Section 3.5 we showed that we achieved a maximum of 10.1% and 5.6% useful yield when ionizing from the $^3F_2$ or the $^3F_3$ states, respectively. For an oxide free surface, we do not expect significant loss of titanium neutrals to states outside the ^{3}F multiplet,[20] nor do we expect losses to TiO_x. Using our prediction for the population of the $^3F_4$, which we cannot measure directly since we could not saturate the transition, we can calculate a maximum theoretical useful yield from the ground state multiplet of $\sim$ 18%. This value is significantly lower than the useful yield of 38% that was measured for uranium metal on the same instrument.[17]

The mean velocity $\bar{v}$ of sputtered atoms for many metals has been demonstrated to be:[21,26,27]

$$\bar{v} = \frac{4}{\pi} \cdot \sqrt{\frac{U_0}{m}} \qquad (2)$$

Here U_0 is the binding energy and m the mass of the atom. The mass difference between titanium and uranium would thus alone predict a higher velocity of sputtered titanium of a factor of 2.2. For a clean titanium metal surface, Dullni[20] used a binding energy of 4.6 eV, which is close to the tabulated heat of sublimation of titanium.[28] Using a binding energy of 5.4 eV for uranium,[21,29,30] we can determine a total velocity difference between sputtered titanium and sputtered uranium of a factor of 2.1. For the sake of simplicity, assuming a spherical expansion of the plume of neutrals above the sample after the sputtering event, the plume of neutral titanium will be twice the diameter of the plume of neutral uranium at any given time. Further assuming that the ionization lasers ionize a cylindrical section through the center of these spheres of neutral atoms and that the delay time between the sputtering and ionization event are identical, we would expect that about twice as many neutrals of uranium

compared to titanium are ionized. While this is a crude approximation it shows that a difference in useful yields between titanium and uranium of roughly a factor of two is expected and primarily due to the difference in mass.

5 Conclusions

We developed a new resonance ionization scheme (Figure 1) for titanium using three tunable Ti:Sa lasers. All three states in the ground state multiplet are populated by sputtering. The transitions from the two lower states ($^3F_2$, $^3F_3$) can be saturated, but the third ($^3F_4$) cannot.

We found nine titanium AI states between 56844 cm^{-1} and 56571 cm^{-1}, for which we give approximate peak widths in Table 1. For our purposes we selected the lowest lying AI state as our ionization transition. This AI transition can be saturated at low irradiance and gives stable isotope ratios, making the scheme suitable for future isotope ratio measurements. Angular momentum selection rules allow us to assign a total angular momentum of the AI state of $J = 3$ or $J = 5$.

The population of the first excited $^3F_3$ state relative to that of the $^3F_2$ ground state is 0.56. Since we could not saturate the $^3F_4 \rightarrow {}^3G_3$ transition, we could not determine the relative population of this state experimentally, however, we estimate its population relative to the ground state as 0.25 by fitting the population using a Boltzmann distribution. This gives the multiplet populations as 55%, 36%, and 14%. The useful yields using a total of three ionization lasers for the $^3F_2$ and $^3F_3$ states was $10.1\% \pm 1.6\%$ and $5.6\% \pm 0.8\%$, respectively. Using the calculated population of the $^3F_4$ state and assuming that almost all of the neutral atoms are in the ground state multiplet we estimate that a total useful yield of $\sim 18\%$ could be achieved if simultaneous saturated ionization from all three ^3F ground states were possible, i.e., a five color scheme. This number is roughly a factor of two lower than for uranium,[17] which agrees with expectations based on the mass difference of sputtered titanium and uranium.

Even when using three lasers to ionize titanium from the ground state, our RIMS measurements show that the presented capability represents a significant improvement for the measurement of presolar stardust. For example, if we assume a SiC grain with 1 μm diameter and a titanium concentration of 4000 ppm by weight – a conservative assumption[31] – we expect an uncertainties in titanium isotope ratio measurements of < 2‰. This is a significant increase in precision over previous measurements of such samples.[5,8] In addition, the presented methods will allow us to also measure smaller stardust grains, e.g., presolar grains of grain types other than SiC, as well as samples with much lower concentrations, enabling a better view into galactic chemical evolution.

Conflicts of interest

There are no conflicts of interest to declare.

Acknowledgements

This work was performed under the auspices of the U.S. Department of Energy by Lawrence Livermore National Laboratory under Contract DE-AC52-07NA27344 and was supported by the Laboratory Directed Research and Development Program at LLNL under project 18-ERD-016. LLNL-JRNL-756574

Notes and references

1 K. Lodders, *The Astrophysical Journal*, 2003, **591**, 1220–1247.
2 K. Lodders, H. Palme and H.-P. Gail, in *Abundances of the Elements in the Solar System*, ed. J. E. Trumper, Springer-Verlag Berlin Heidelberg, 2009, ch. 4.4, pp. 560–630.
3 A. M. Davis, *Proc. Natl. Acad. Sci.*, 2011, **108**, 19142–19146.
4 E. Zinner, *Meteorites and Cosmochemical Processes*, Oxford, Vol. 1 Treatise on Geochemistry 2nd Ed. (exec. eds. H. D. Holland and K. K. Turekian), Elsevier, 2014, pp. 181–213.
5 C. M. O'D. Alexander and L. R. Nittler, *The Astrophysical Journal*, 1999, **519**, 222–235.
6 J. Levine, M. R. Savina, T. Stephan, N. Dauphas, A. M. Davis, K. B. Knight and M. J. Pellin, *Int. J. Mass Spectrom.*, 2009, **288**, 36–43.
7 R. Trappitsch, T. Stephan, M. R. Savina, A. M. Davis, M. J. Pellin, D. Rost, F. Gyngard, R. Gallino, S. Bisterzo, S. Cristallo and N. Dauphas, *Geochimica et Cosmochimica Acta*, 2018, **221**, 87–108.
8 A. N. Nguyen, L. R. Nittler, C. M. Alexander and P. Hoppe, *Geochimica et Cosmochimica Acta*, 2018, **221**, 162–181.
9 R. L. Hervig, F. K. Mazdab, P. Williams, Y. Guan, G. R. Huss and L. A. Leshin, *Chemical Geology*, 2006, **227**, 83–99.
10 N. Liu, M. R. Savina, R. Gallino, A. M. Davis, S. Bisterzo, F. Gyngard, F. Käppeler, S. Cristallo, N. Dauphas, M. J. Pellin and I. Dillmann, *Astrophys. J.*, 2015, **803**, 12 (23pp).
11 J. G. Barzyk, M. R. Savina, A. M. Davis, R. Gallino, F. Gyngard, S. Amari, E. Zinner, M. J. Pellin, R. S. Lewis and R. N. Clayton, *Meteoritics & Planetary Science*, 2007, **42**, 1103–1119.
12 D. R. Spiegel, W. F. Calaway, A. M. Davis, J. W. Burnett, M. J. Pellin, S. R. Coon, C. E. Young, R. N. Clayton and D. M. Gruen, *Analytical Chemistry*, 1992, **64**, 469–475.
13 R. K. Wunderlich, G. J. Wasserburg, I. D. Hutcheon and G. A. Blake, *Analytical Chemistry*, 1993, **65**, 1411–1418.
14 M. R. Savina, M. J. Pellin, E. C. Tripa, I. V. Veryovkin, W. F. Calaway and A. M. Davis, *Geochim. Cosmochim. Acta*, 2003, **67**, 3215–3225.
15 T. Stephan, R. Trappitsch, A. M. Davis, M. J. Pellin, D. Rost, M. R. Savina, R. Yokochi and N. Liu, *Int. J. Mass Spectrom.*, 2016, **407**, 1–15.
16 M. R. Savina, B. H. Isselhardt, A. Kucher, R. Trappitsch, B. V. King, D. Ruddle, R. Gopal and I. Hutcheon, *Analytical Chemistry*, 2017, **89**, 6224–6231.
17 M. R. Savina, B. H. Isselhardt and R. Trappitsch, *Analytical Chemistry*, 2018, http://dx.doi.org/10.1021/acs.analchem.8b02656.
18 V. S. Letokhov, *Laser Photoionization Spectroscopy*, Academic Press, Inc., 1987.
19 P. Boehnke, E. A. Bell, T. Stephan, R. Trappitsch, C. B. Keller, O. S. Pardo, A. M. Davis, T. M. Harrison and M. J. Pellin, *Proceedings of the National Academy of Sciences*, 2018, **115**, 6353–6356.

20 E. Dullni, *Applied Physics A*, 1985, **38**, 131–138.
21 R. Wright, M. Pellin, D. Gruen and C. Young, *Nuclear Instruments and Methods*, 1980, **170**, 295–302.
22 M. R. Savina, R. Trappitsch, A. Kucher and B. H. Isselhardt, *Spectrochimica Acta Part B*, 2018, accepted.
23 A. Müller and A. Benninghoven, *Surface Science*, 1974, **41**, 493–503.
24 S. Hayashi and N. Kubota, *Applied Surface Science*, 2008, **255**, 834–836.
25 A. Cortona, W. Husinsky and G. Betz, *Physical Review B*, 1999, **59**, 15495–15505.
26 E. Hintz, D. Rusbüldt, B. Schweer, J. Bohdansky, J. Roth and A. Martinelli, *Journal of Nuclear Materials*, 1980, **93-94**, 656–663.
27 H. Bay, B. Schweer, P. Bogen and E. Hintz, *Journal of Nuclear Materials*, 1982, **111-112**, 732–737.
28 J. Rumble, *Handbook of Chemistry and Physics*, CRC Press, 2018.
29 R. A. Weller and T. A. Tombrello, *Radiation Effects*, 1978, **37**, 83–92.
30 C. E. Young, R. B. Cohen, P. M. Dehmer, L. G. Pobo and S. Wexler, *The Journal of Chemical Physics*, 1976, **65**, 2562–2567.
31 S. Amari, P. Hoppe, E. Zinner and R. S. Lewis, *Meteoritics*, 1995, **30**, 679–693.